JOURNAL OF CATALYSIS 109, 367–377 (1988)

Structural Characterization of Malachite-like Coprecipitated Precursors of Binary CuO–ZnO Catalysts

PIERO PORTA, SERGIO DE ROSSI, GIOVANNI FERRARIS, MARIANO LO JACONO, GIULIANO MINELLI, AND GIULIANO MORETTI

Centro su "Struttura e Attività Catalitica di Sistemi di Ossidi" (SACSO) del CNR, c/o Dipartimento di Chimica, Università di Roma "La Sapienza," Piazzale Aldo Moro 5, 00185 Rome, Italy

Received April 22, 1987; revised August 14, 1987

Copper and zinc hydroxycarbonates with Cu/Zn atomic ratios of 100/0, 92/8, 85/15, 77/23, 67/33, and 50/50 were prepared by the coprecipitation method. The samples with the ratios 100/0, 92/8 and 85/15 were monophasic with the monoclinic $P2_1/a$ malachite structure, whereas the richer zinc samples contained in addition to the malachite phase the orthorhombic $B22_12$ aurichalcite, whose concentration was very low in the 77/23 specimen but increased continuously with zinc content. The amount of aurichalcite in the biphasic powders has been estimated by means of quantitative X-ray diffraction and differential thermal analysis. With only those X-ray reflections belonging to the malachite structure taken into account, the unit cell constants for all the solid solution hydroxycarbonates have been determined, showing that as a whole the cell volume of malachite decreases continuously with increasing zinc content. This result is related, as shown also by DTA measurements and thermochemical literature data, to an increasing stability of compounds richer in zinc, to increasing covalent effects, and/or to less octahedral site distortion around the metal atoms when zinc substitutes for Cu^{2+} ions in the malachite lattice. Magnetic susceptibility and thermogravimetric measurements together with diffuse reflectance spectra are also presented and discussed.

INTRODUCTION

Catalysts for the methanol synthesis and CO conversion reactions based on mixed oxides containing copper, zinc, and aluminum (or chromium) have received a great deal of attention owing to their ability to perform these industrial processes at temperatures and pressures much lower (*1–4*) than the catalysts based on ZnO/Cr_2O_3 previously used (*5*).

Despite the importance of this class of catalysts and the considerable amount of work on them that has appeared in the literature, the exact nature of the geometrical and oxidation-state changes occurring during catalyst function has yet to be unraveled. Particularly important in CuO–ZnO–Al_2O_3 (or Cr_2O_3) based catalysts is the role played by reduced copper and its interaction with ZnO. While some authors (*6–8*) claim that this interaction gives rise to a synergic effect, i.e., the binary catalyst is much more active than the each component on its own, more recent work (*9, 10*) casts doubts on the Cu/ZnO synergy, pointing out that only the copper surface is involved in the rate-determining step of the synthesis. Hence the role of ZnO in the industrial catalyst is still a matter of debate.

Given the importance of obtaining mixed oxide systems with high component interdispersion, there is still considerable interest in finding preparative methods capable of giving precursors having all metals in a single crystalline phase. The most promising preparation method for such multicomponent catalysts satisfying all requirements is the coprecipitation technique, by which a precursor, namely a hydroxycarbonate, is made, in which all the elements are in the same structure.

Preparation methods for CuO/ZnO catalysts have been described in several of the

0021-9517/88 $3.00

papers cited above, and there is also an extensive patent literature on this system, which can be found in Ref. (*1*).

For the binary systems CuO–ZnO, coprecipitated hydroxycarbonate precursors with less than 30% copper consist of mixtures of hydrozincite [$Zn_5(CO_3)_2(OH)_6$] and aurichalcite [$(Cu_xZn_{1-x})_5(CO_3)_2(OH)_6$] (*4*), whereas with a copper content equal to 30%, monophasic precursors with hydrozincite (*11*) or with aurichalcite (*4*) structures have been reported. When Cu/Zn atomic ratios are higher than 30/70, mixtures of hydrozincite, malachite [$Cu_2CO_3(OH)_2$], aurichalcite, and rosasite [$(Cu,Zn)_2CO_3(OH)_2$] have been found (*12, 13*).

However, even though it has been noted that hydrozincite and malachite may each form solid solutions containing the other metal (*12, 13*), no systematic structural study of zinc-containing malachites has hitherto appeared in the literature.

Investigations have therefore been undertaken in our laboratory to elucidate the following points: stability of formation of mixed hydroxycarbonate precursors rich in copper, i.e., with Cu/Zn atomic ratios in the range 100/0–50/50; the limit of solubility of zinc in the malachite structure; and the structural and catalytic properties of CuO/ZnO mixed oxides. The present paper reports the results of the preparation of the zincian–malachite precursors and their structural features. The study of the hydroxycarbonates' decomposition to CuO/ZnO, of their behavior to reduction under hydrogen, and of their catalytic activity during hydrogenation reactions is in progress.

EXPERIMENTAL

Sample preparation and analysis. Precursors with nominal atomic ratios of Cu/Zn = 100/0, 92/8, 85/15, 77/23, 67/33, and 50/50 were prepared by coprecipitation at constant pH = 8 from Cu, Zn nitrate solutions in suitable proportions with $NaHCO_3$, a method similar to that already described (*3*). In particular, 0.5 liter of a 1 *M* aqueous solution of C. Erba reagent grade Cu and Zn nitrates was rapidly added to 1 liter of a 1.2 *M* aqueous solution of $NaHCO_3$ heated to 333–343 K under vigorous stirring. This reverse precipitation procedure adopted for all the samples using a rather large excess of sodium bicarbonate ensured the constancy of the pH during the operation. A pale blue precipitate was immediately formed which, under stirring and heating at the same temperature, changed after a certain time (variable from 5 to 110 minutes depending on the different compositions), to deep green. The change itself was rapid (1–2 min). The green precipitate was then left under continuous stirring at 333–343 K for another 90 min; the hot dispersion was then filtered and the solid mass was washed many times with cold distilled water and finally dried at 363 K overnight.

The hydroxycarbonate with Cu/Zn = 30/70, aurichalcite, used for quantitative X-ray diffraction and DTA determination, was prepared by coprecipitation of Cu, Zn nitrates following procedures described in the literature (*4, 11*). After slow addition of a 1 *M* aqueous solution of Na_2CO_3 at 333 K to a solution of Cu and Zn nitrates in suitable proportions, the precipitate obtained was filtered, washed with hot distilled water for 2 h, and dried at 393 K overnight. The color of this sample was pale blue. Since the X-ray pattern of the prepared solid resembled that of hydrozincite (*14*) and gerhardtite (*15*), the dried compound was retreated with a 1 *M* aqueous solution of $NaHCO_3$ at 333 K for 2 h under stirring. As a result, the color of the precipitate changed from pale blue to pale blue-green. After filtering, washing with hot distilled water for 2 h, and drying at 393 K overnight, the X-ray powder spectrum of the dried sample was practically identical to that described in Ref. (*4*) and assigned to a predominantly single-phase aurichalcite (*14*).

Elemental copper and zinc analyses were performed by the atomic absorption tech-

TABLE 1

Nominal and Experimental Percentages of Copper and Zinc, Nominal and Experimental Weight Losses, Maximum Temperature Peaks (K) drawn from DTA, and Percentages of the Phases Present for the Cu/Zn Catalyst Hydroxycarbonate Precursors

Sample (Cu/Zn)	Chemical analysis[a]				Thermal analysis					Phases[b] present (%)				
					TGA		DTA			DTA			X-ray	
	Cu% nom.	Cu% exp.	Zn% nom.	Zn% exp.	% w.l. nom.	% w.l. exp.	T'_{max}	T''_{max}	T'''_{max}	M	A	H	M	A
100/0	57.48	53.0			28	29	578			100			100	
92/8	52.81	50.1	4.72	4.29	28	29	613			100			100	
85/15	48.73	46.7	8.84	7.85	28	30	628			100			100	
77/23	44.09	42.3	13.55	12.3	28	28	633	593		90	10		89	11
67/33	38.30	41.8	19.41	19.2	28	28	638	613		60	40		66	34
50/50	28.50	28.9	29.33	25.3	28	28	643	608		10	80	10		
0/100			58.17	57.6	26	24			518					

[a] By atomic absorption.
[b] M, malachite; A, aurichalcite; H, hydrozincite.

nique with a Varian SpectrAA-30 instrument.

Table 1 reports the nominal and experimentally observed Cu and Zn contents. The nominal percentages of Cu and Zn reported in Table 1 for all the samples refer to what was expected from the composition and volumes of the solutions used for precipitation and on the basis of the formula $(Cu_{1-x}Zn_x)_2CO_3(OH)_2$.

X-ray diffraction. The powder diffraction patterns were obtained with a Philips automated PW 1729 diffractometer. Scans were taken with a 2θ step size of 0.01°, using Cu $K\alpha$ (nickel-filtered) radiation. The intensities of the reflections were estimated by evaluation of the integrated peaks. Structural data for several reference hydroxycarbonates were taken from the literature (*14, 16, 17*).

Quantitative amounts of aurichalcite present in the samples Cu/Zn = 77/23 and 67/33 (see below) were determined from the integrated intensities of the (120) reflection of malachite (2θ = 17.5°) and of the (400) reflection of aurichalcite (2θ = 13°). Two methods were used for this purpose: first, preparation of mechanically mixed standards of the pure malachite (Cu/Zn = 100/0) and aurichalcite (Cu/Zn = 30/70) at variable and known contents of aurichalcite and determination of the amount of aurichalcite from the calibration curve by comparing the relative intensities, and second, mechanical preparation of mixtures of the precursors 77/23 and 67/33 with aurichalcite at different weight ratios and use of the calibration curve to compare the relative integrated reflection intensities of the samples under study. The reproducibility of the two methods was within 10%. The average values of the relative amounts of malachite and aurichalcite drawn from the two methods are reported in Table 1. The sample with Cu/Zn = 50/50 was not analyzed by this procedure owing to its low crystallinity and because DTA measurements, as shown below, indicated the presence of a small amount of hydrozincite.

Reflectance spectra. Diffuse reflectance spectra were taken in the wavelengths range 350–2500 nm with a Beckman DK-1A spectrometer equipped with a diffuse reflectance accessory, using MgO as the reference.

Magnetic susceptibility. Magnetic sus-

ceptibilities were measured by the Gouy method over the temperature range 100–300 K. Correction was made for the diamagnetism of the sample. A check that the susceptibilities were independent of magnetic field strength was made. One sample, namely Cu/Zn = 100/0, was also tested at liquid helium temperature in the laboratory at the Istituto ITSE (CNR), Area della Ricerca, Montelibretti, Rome, through the courtesy of Dr. D. Fiorani.

Thermal analysis. Thermogravimetric determinations (TGA) were carried out under a flow of N_2 (24 cm^3 min^{-1}) with a Cahn RG electrobalance, using 10–13-mg samples contained in a silica bucket. The temperature was raised from room temperature to 773 K by a linear programmer at a heating rate of 5 K min^{-1}. The weight was measured to within an accuracy of 0.04 mg. Differential thermal analysis (DTA) was performed with a Perkin–Elmer 1700 instrument connected to a Perkin–Elmer system 7/4 thermal analysis controller. The sample weight was 14–16 mg and α-Al_2O_3 was used as reference. The analysis was run at 5 K min^{-1} from room temperature to 773 K under a N_2 flow of 50 cm^3 min^{-1}.

RESULTS

X-ray diffraction. The X-ray powder spectra showed that all the compounds studied except Cu/Zn = 50/50 are highly crystalline. As shown in Table 2, there is very close similarity between the natural malachite (*17*) and our copper hydroxycarbonate 100/0 preparation. Also, the zinc-containing copper precursors are isomorphous with the pure copper hydroxycarbonate, as shown in Table 2, where the observed d_0 spacings and the relative intensities of the diffraction lines belonging to the malachite structure are reported for all the Cu/Zn compounds prepared.

A careful inspection of the d_0 values drawn from all the Cu/Zn precursors has indeed revealed that whereas no systematic variation in the position of the peaks occurs for some classes of *hkl* reflections, namely those where $l = 0$, the reflections where $l \neq 0$ show on the contrary some interesting and systematic displacements. The d_0 spacings of the reflections having negative and positive l continuously decrease and increase, respectively, with increasing Zn content.

It was interesting to clarify these observations by adopting the following procedure. The Miller indices of the reflections belonging to the malachite monoclinic structure were introduced into the formula (*18*)

$$1/d^2_{hkl} = h^2a^{*2} + k^2b^{*2} + l^2c^{*2} \pm 2hla^*c^* \cos \beta^*, \quad (1)$$

where $a^* = 1/(a \sin \beta)$, $b^* = 1/b$, $c^* = 1/(c \sin \beta)$, and $\beta^* = 180° - \beta$ are the reciprocal cell parameters. By trial and error the best fit between observed and calculated $1/d^2$ values was obtained. The real lattice parameters a, b, c β, and the cell volume V were thus defined for each sample. The calculated d values and the cell parameters are reported in Tables 2 and 3, respectively. Values of the volume of the cell for all the precursors are also shown in Fig. 1.

Table 3 shows that with increasing Zn content, a, c, and β decrease, b increases, and as a whole the cell volume V decreases. It may be noted that a similar behavior was observed by Jambor (*19*) in zincian–malachite minerals with Zn/Cu ratios up to 0.3. In the light of these results it is not surprising that mixed reflections where $l = 0$, namely the *hk*0, and whose positions are not strongly influenced from the opposite trend of a and b do not show a systematic shift in d_0, whereas the *h*0*l* and *hkl* reflections systematically feel the influence of the last term in Eq. (1). In fact, for the *h*0*l*–*hkl* and $\bar{h}$0*l*–$\bar{h}kl$ pairs of reflections, the positive or negative $2hla^*c^* \cos \beta^*$ term, respectively, causes a systematic displacement in the observed direction. It may be noted from Table 2 that some reflections with a nearly constant intensity, close in the spec-

TABLE 2

Intensities, d-Spacings (Å), and Miller Indexes from Mineral Malachite,[a] Intensities,[b] Observed and Calculated d-Spacings for Cu/Zn Catalyst Hydroxycarbonate Malachite-Like Precursors

Malachite			Cu/Zn:100/0			Cu/Zn:92/8			Cu/Zn:85/15			Cu/Zn:77/23			Cu/Zn:67/33			Cu/Zn:50/50		
I	d_o	hkl	I	d_o	d_c	I	d_o	d_c	I	d_o	d_c	I	d_o	d_c	I	d_o	d_c	I	d_o	d_c
12	7.41	110	6	7.42	7.41	6	7.41	7.41	5	7.41	7.40	5	7.41	7.39						
55	5.993	020	35	5.99	5.98	28	6.02	6.02	33	6.014	6.020	30	6.049	6.047	30	6.046	6.046	10	6.03	6.03
75	5.055	120	55	5.047	5.045	46	5.067	5.070	55	5.059	5.060	60	5.073	5.073	60	5.076	5.076	20	5.06	5.07
14	4.699	200	10	4.703	4.704	5	4.703	4.704	11	4.683	4.683	9	4.671	4.671	15	4.676	4.676	6	4.65	4.67
85	3.693	220	60	3.690	3.695	55	3.696	3.705	66	3.690	3.695	70	3.693	3.695	70	3.693	3.698	70	3.69	3.69
18	3.028	310	13	3.033	3.033	14	3.026	3.034	20	3.013	3.022	20	3.023	3.017	25	3.015	3.019	6	3.01	3.02
18	2.988	040	13	2.985	2.988	10	2.998	3.010			3.010			3.021			3.020			3.02
100	2.857	$\bar{2}01$	100	2.860	2.863	100	2.833	2.826	100	2.810	2.814	100	2.792	2.790	100	2.788	2.786	80	2.78	2.78
		140			2.848			2.866			2.865			2.878			2.875			2.88
40	2.823	111	40	2.833	2.824			2.825			2.824			2.820			2.819			2.81
		021			2.830			2.822			2.818			2.808			2.806			2.80
45	2.778	320	40	2.782	2.777	36	2.757	2.781	38	2.736	2.771	40	2.721	2.771	50	2.718	2.771	40	2.73	2.77
		$\bar{2}11$			2.784			2.751			2.740			2.719			2.715			2.71
55	2.520	240	40	2.520	2.522	27	2.527	2.533	33	2.529	2.532	32	2.536	2.537	30	2.534	2.537	10	2.53	2.54
30	2.477	201	24	2.479	2.482	22	2.489	2.491	30	2.488	2.488	36	2.491	2.490	35	2.491	2.490	10	2.49	2.49
35	2.464	330	16	2.461	2.464	13	2.465	2.471	10	2.465	2.464	15	2.460	2.462	20	2.468	2.466	10	2.46	2.47
20	2.425	211	13	2.433	2.430	13	2.438	2.439	17	2.438	2.437	23	2.439	2.439	25	2.442	2.439	15	2.45	2.44
14	2.349	400	11	2.350	2.352	10	2.344	2.352	17	2.338	2.342	20	2.335	2.336	25	2.335	2.339	10	2.33	2.34
		131			2.349			2.355			2.353			2.351			2.350			2.35
18	2.316	$\bar{2}31$	11	2.309	2.325	8	2.324	2.316	14	2.299	2.304	16	2.302	2.296	18	2.302	2.291	10	2.29	2.29
18	2.289	221	10	2.292	2.292	10	2.301	2.301			2.299			2.302			2.302			2.30
		041			2.187			2.190			2,189			2.189			2.187			
20	2.186	420	10	2.186	2.188	10	2.188	2.190	13	2.183	2.182	14	2.183	2.180	12	2.185	2.181			
		$\bar{1}41$			2.181			2.179			2.176			2.175			2.174			
20	2.129	250	11	2.129	2.131	10	2.135	2.143	10	2.139	2.141	7	2.144	2.146	15	2.145	2.147	16	2.14	2.15
18	2.076	$\bar{3}31$	16	2.065	2.077	18	2.063	2.064	20	2.056	2.056	15	2.047	2.046	15	2.044	2.044	8	2.04	2.04
10	2.054	311	8	2.054	2.059	8	2.059	2.061	8	2.067	2.066	8	2.069	2.067	8	2.071	2.071	4	2.07	2.07
12	1.991	060	4	1.991	1.992	3	1.997	2.002												
18	1.969	321	10	1.973	1.974	12	1.979	1.983	11	1.979	1.981	12	1.983	1.983	12	1.984	1.984	4	1.98	1.98
16	1.947	160	10	1.941	1.949	5	1.957	1.962	5	1.959	1.962	5	1.958	1.962	5	1.958	1.962	8	1.95	1.96
10	1.941	$\bar{4}21$			1.941			1.926			1.916			1.912			1.903			1.90
18	1.911	151	10	1.905	1.916	14	1.918	1.922	17	1.908	1.912	14	1.908	1.910	15	1.907	1.910	10	1.91	1.91
		241			1.911			1.919			1.918			1.918			1.919			1.92
10	1.833	$\bar{2}51$	5	1.834	1.837	5	1.839	1.834	2	1.845	1.830	2	1.850	1.840						
25	1.691	$\bar{1}61$	13	1.684	1.691	13	1.682	1.693	8	1.689	1.692	7	1.692	1.693	5	1.692	1.693	8	1.69	1.69
14	1.678	450			1.678			1.682	10	1.675	1.679	9	1.667	1.678	8	1.675	1.678	5	1.67	1.68

[a] From Ref. (*17*).
[b] From integrated peaks.

tra but different in the sign of the h index, are displaced in such a way that when Zn content increases, they invert the relative position (for instance the $\bar{3}31$ with 311), and others, such as the 111 and 221, no longer appear in the more Zn-rich malachites since they are superimposed on the preceding reflections $\bar{2}01$ and $\bar{2}31$, respectively.

The most relevant term influencing the observed displacement of the hkl reflections appears to be the angle β, whose decrease with increasing zinc content makes the cell closer to an orthorhombic lattice, as found in aurichalcite (*14*).

TABLE 3

Lattice Constants for the Cu/Zn Hydroxycarbonate Malachite-Like Precursors of Catalysts

Sample (Cu/Zn)	a (Å)	b (Å)	c (Å)	β	V (Å^3)
100/0	9.518	11.947	3.249	98°45′	365.16
92/8	9.495	12.034	3.224	97°48′	364.48
85/15	9.444	12.034	3.217	97°30′	362.48
77/23	9.416	12.077	3.201	97°	361.28
67/33	9.414	12.077	3.190	96°55′	360.05
50/50	9.412	12.077	3.187	96°48′	359.71

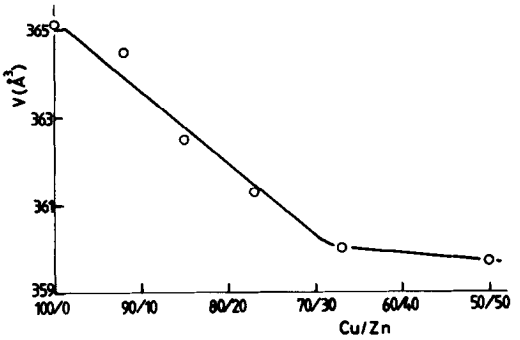

FIG. 1. Cell volume vs Cu/Zn atomic ratios for zincian–malachite hydroxycarbonates.

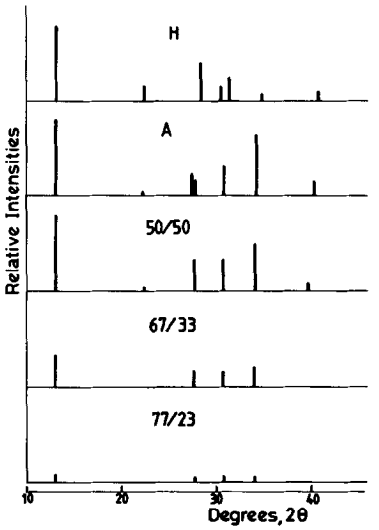

FIG. 2. Extra lines, in addition to those belonging to the malachite structure, from X-ray powder diffraction spectra of Cu/Zn hydroxycarbonate precursors richer in zinc. Corresponding lines for aurichalcite, A, and hydrozincite, H from Ref. (*14*) are also shown.

For the most concentrated Zn precursors, i.e., those with Cu/Zn atomic ratios of 77/23, 67/33, and 50/50, some extra lines other than those belonging to the malachite structure shown in Table 2 are present in the X-ray spectra. These lines, which are shown in Fig. 2, are very weak in the 77/23 sample and increase in intensity with increasing Zn content in such a way that the first one at $2\theta = 13.1°$ becomes the strongest reflection in the whole X-ray pattern of the 50/50 sample. They are indicative of an increasing formation of a new phase which, according to the present literature (*4, 11*) may be aurichalcite or hydrozincite. However, a careful inspection of the relative intensities (see Fig. 2) leads to the conclusion that the extra phase is indeed aurichalcite. In fact, the intensity sequence found in the 50/50 sample, which is repeated with nothing more than a change of scale in the other two compounds, is equal to 100, 40, 40, and 60 for the reflections at $2\theta = 13.1$, 27.8, 30.8, and 34.1°, respectively; this is more in agreement with the sequence reported for aurichalcite (100, 30 + 20, 40, 80) than for hydrozincite (100, 50, 20 + 30, 10).

Thermal analysis. The weight losses found from TGA measurements and reported in Table 1 agree fairly well with those expected for the decomposition of hydroxycarbonates, $M_2CO_3(OH)_2$, to oxides. For the most Zn-dilute precursors (Cu/Zn = 100/0, 92/8, and 85/15) as well as for the pure hydrozincite the thermogravimetric curves (Fig. 3) indicate a single narrow decomposition from monophasic pre-

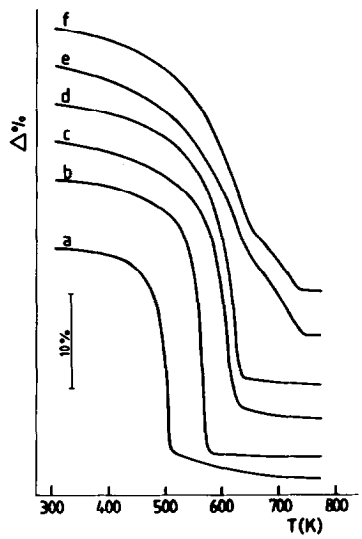

FIG. 3. Weight losses vs temperature (K) from TGA measurements for Cu/Zn hydroxycarbonate precursors (a = 0/100; b = 100/0; c = 92/8; d = 85/15; e = 77/23; f = 67/33). The scale amount for 10% weight loss is also reported.

cursors (curves a, b, c, and d) that starts at a temperature around 423 K and ends at about 600 K; on the other hand, for the Cu/Zn = 77/23 and 67/33 precursors (curves e and f of Fig. 3), the curves are smoother and seem to indicate a two-stage decomposition. The DTA curves are shown in Fig. 4. Table 1 reports the maximum peak temperatures for each sample. Pure malachite decomposes in the range 550–600 K with a sharp maximum at 578 K. When zinc is added, (up to Cu/Zn = 85/15) the thermal decomposition range is broadened and an increasing shift of the maximum peak toward higher temperatures is observed. The DTA curves of the more Zn-rich precursors (Cu/Zn = 77/23, 67/33, and 50/50) show, however, two distinct peaks: that at higher temperature and whose peak temperature increases with increasing zinc content (from 633 to 643 K) is assigned to the zincian–malachite on the basis of the trend observed for the monophasic preceding precursors, whereas the other one appearing in the range 603–613 K cannot be assigned to a copper–hydrozincite phase since, as shown in Fig. 4, the pure hydrozincite (curve h) decomposes at much lower temperature (~518 K). The latter peak is probably attributable to a copper-containing zinc hydroxycarbonate with an aurichalcite-like phase, as inferred from the results obtained by Petrini *et al.* (*11*) and from the comparison with the thermogram produced by the pure aurichalcite (curve g of Fig. 4). It may be noted that the specimen with 50% of zinc also shows a small maximum at about 513 K, which can be assigned to a slight amount of pure hydrozincite.

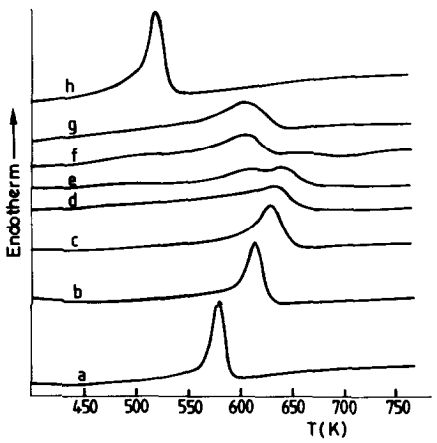

FIG. 4. Endothermic peaks vs temperature (K) from DTA measurements for Cu/Zn hydroxycarbonate precursors (a = 100/0; b = 92/8; c = 85/15; d = 77/23; e = 67/33; f = 50/50; g = 30/70; h = 0/100).

Concerning the relative amounts of the different precursors, malachite and aurichalcite, present in the more zinc-rich samples, an accurate calculation from the DTA measurements must involve knowledge of the exact position of the maxima, the shape of the peak and of the background, the decomposition enthalpy, and the thermal conductivity of the single phases. However, a rough estimation has been attempted and the results are summarized in Table 1 for those samples (77/23 and 67/33) where only two phases (malachite and aurichalcite) were present. Table 1 also reports the relative amounts of malachite, aurichalcite, and hydrozincite present in the 50/50 specimen.

Reflectance spectroscopy. The reflectance spectra of all the precursors show a large band centered at about 810 nm (12,350 cm^{-1}) with a shoulder at about 1150 nm (8,700 cm^{-1}).

Magnetic susceptibility. The effective magnetic moments, μ, for all the compounds are found to be in the range 1.8–2.1 B.M. The pure malachite (100/0) tested at liquid helium temperature gave a magnetic moment of 1.7 B.M. The Weiss temperature, Θ, has a value of -150 K for the 100/0 sample and decreases with increasing zinc content.

DISCUSSION

The mineral malachite is monoclinic, a = 9.502, b = 11.974, c = 3.24 Å, β = 98°45′, space group $P2_1/a$; its structure has been determined by Wells (*17*), who found a distorted octahedral coordination around cupric ions. The copper atoms within the molecule are nonequivalent: Cu_I is surrounded

by four oxygen atoms belonging to CO_3 groups and two OH ions, Cu_{II} by two oxygen atoms of the carbonate anion and four OH ions. Both Cu_I and Cu_{II} distorted octahedra form strings in the *c* direction linked by edges. The mean values of the four coplanar and two apical interatomic Cu–O distances for Cu of type I are 1.98 and 2.71 Å, and for Cu of type II are 2.01 and 2.41 Å, respectively, an interesting example of the type of tetragonally elongated octahedral coordination to be expected for Cu^{2+} (*20*).

It is interesting to notice that in the mineral tenorite, CuO, an essentially covalent crystal with monoclinic structure and which is the expected oxide product of malachite decomposition, the copper atoms lie between four oxygens nearly in a plane at the corners of a square. The four coplanar Cu–O bonds have a length of 1.95 Å (*21*), closely similar to that of the shorter bonds in the malachite structure.

Zinc can be doped into the malachite lattice, giving zincian–malachites (*12, 13, 19*); however, as more and more zinc is added, other phases are formed, namely aurichalcite (*4*) and copper hydrozincite (*9*).

Our study has demonstrated definitively that, at least up to 15% of zinc (Table 2), monophasic precursors with a malachite structure are formed. The X-ray lines of the 100/0 compound, as well as those for the 92/8 and 85/15 compositions, can be indexed as belonging to the monoclinic malachite structure (*17*).

For the specimens with zinc content higher than 15%, in addition to the zinc-containing malachite phase, a new phase richer in zinc, i.e., aurichalcite, as shown in Fig. 2, starts to segregate. However, the increasing zinc concentration not only gives rise to the segregation of aurichalcite but also permits further solubility of zinc into the malachite lattice. As shown in Fig. 1, the decrease of the malachite cell volume with increase zinc content is still evident up to about 30% of zinc, a value which may be estimated as the limit of solubility.

The decrease of the cell volume of the zincian–malachites with increasing zinc content seems indeed in contrast with expectations based only on the isomorphous substitution of Cu^{2+} by Zn^{2+} ions within the malachite lattice, since the octahedral ionic radii for Cu^{2+} and Zn^{2+} are 0.73 and 0.74 Å, respectively (*22*). However, this behavior may be explained by an increasing covalency of the metal–oxygen bonds and/or by less octahedral site distortion around the metal atoms when zinc substitutes for the copper ions, both effects leading to lattice shrinking and higher stability of the zincian–malachites than of the pure copper hydroxycarbonate. It is most likely that Zn preferentially enters one of the two nonequivalent copper environments, probably the less octahedrally distorted (type II) metal site in the monoclinic malachite structure. The higher structural stability of zincian–malachites seems in contrast with the observed limit of solubility of zinc (30%) and with the appearance of a new phase, aurichalcite, which in its proposed complex sheet structure (*23*) contains 60% octahedral and 40% tetrahedral sites for the divalent cation. The blue color of the aurichalcite specimens indeed indicates that the Cu^{2+} ions occupy the octahedral holes preferentially, while the tetrahedral holes are most probably occupied by zinc, because of its preference for the latter type of coordination (*20*). It is then not surprising that, beyond a certain limit of solubility of Zn into the malachite lattice, a new phase, where zinc may better satisfy its tetrahedral site preference, is more easily formed, as occurs in copper–zinc minerals (*19*).

The covalent effect, which is shown by a lack of additivity of the ionic radii and is generally referred to as "covalent shortening" (*22*), has already been observed experimentally in some mixed oxide systems where zinc ions are involved, e.g., $Cu_xZn_{1-x}Al_2O_4$ (*24*) and $Co_xZn_{1-x}Al_2O_4$ (*25*), and it may be ascribed to the difference in electron configuration between Zn^{2+} ($3d^{10}$) and other ions, such as Cu^{2+} ($3d^9$), which exhibit more ionic character

with oxygen (*20, 26*). The other cooperative effect, i.e., the decrease of the local octahedral distortion, is also linked to the different electron configuration of zinc and copper ions, the latter having more tendency than zinc to give elongation of the oxygen octahedra (*20*).

The DTA results, Table 1 and Fig. 4, also indicate that the dissolution of zinc in the malachite lattice induces some thermal stabilization of the structure, since the maximum peak temperature (T') assigned to the decomposition of malachite-like phases shifts from 578 to 643 K with increasing zinc content, in agreement with the findings of other authors (*11, 12*). It may be added that the decomposition temperature found for the zinc-free malachite, 100/0, agrees fairly well with the value of 588 K reported in the literature for the mineral malachite, (*27*) and for the synthetic product $Cu_2CO_3(OH)_2$ (*28*).

The TGA measurements (Fig. 3) also point to the formation of monophasic precursors with malachite structures for compounds with atomic ratios Cu/Zn= 100/0, 92/8, and 85/15, which give a one-step decomposition.

The appearance of a broad optical band with a maximum centered at about 810 nm (12,350 cm^{-1}) and a shoulder at about 1150 nm (8,700 cm^{-1}) indicates a distorted octahedral surrounding of oxygens around the copper ions in the malachite structure (*29*).

The magnetic moment, 1.7 B.M., found for the 100/0 sample at liquid helium temperature also confirms the octahedral site symmetry around copper ions. A strong antiferromagnetic interaction among the copper ions, i.e., a Weiss temperature equal to −150 K, is present in the pure copper malachite (100/0). This interaction between paramagnetic ions decreases, as observed in the zincian–malachites, when zinc (diamagnetic ion, $3d^{10}$) substitutes for copper.

For zinc contents higher than 15% another phase in addition to malachite appears, which could be either aurichalcite, A, or a copper hydrozincite, H. In spite of the fact that the orthorhombic $B22_12$ aurichalcite and the monoclinic C2/m hydrozincite are crystallographically distinct (*14*), they have similar XRD powder patterns. However, A can be distinguished from H, as has been demonstrated previously by Himelfarb *et al.* (*4*), by means of a careful comparison of some X-ray reflections appearing in the XRD spectra of these two chemically related compounds; these authors showed that in the XRD patterns reported for a sample at Cu/Zn = 30/70 by Petrini *et al.* (*11*), lines typical of A instead of those of H were surely present.

Since an unambiguous XRD identification of synthetically prepared aurichalcite has not yet been reported in the literature, we have also prepared (see Experimental) a hydroxycarbonate with Cu/Zn = 30/70, whose X-ray powder spectrum is practically identical to that described by Himelfarb *et al.* (*4*) and matches that of aurichalcite (*14*). The synthetic hydrozincite with Cu/Zn = 0/100 has also been prepared.

A comparison between the XRD patterns of the prepared reference compounds A and H and the extra lines appearing in the spectra taken from the precursors richer in zinc (from Cu/Zn = 77/23 down to 50/50) has unambiguously identified the latter ones as belonging to the A phase, Fig. 2. A quantitative XRD analysis of the relative amounts of malachite and aurichalcite is reported in Table 1 for the biphasic samples 77/23 and 67/33.

The XRD results are confirmed by thermoanalysis. From TGA measurements a wider temperature range for decomposition was observed for the samples above than in the Cu/Zn = 100/0, 92/8, and 85/15 samples (Fig. 3), thus indicating that biphasic and monophasic systems are present in the two series. The DTA analysis has further shown that both M and A are present in the samples at Cu/Zn from 77/23 to 50/50. An increasing shift of the endothermic maxima due to malachite (T'_{max} in Table 1) is observed with increasing Zn content, which is

a proof, in agreement with the shrinkage of the cell volume observed by XRD, of a greater structural stability of zincian–malachites with respect to pure malachite. The increasing thermal stability of the copper hydroxycarbonates with increasing zinc content could also be inferred from the extrapolation of the standard free energies of formation, $\Delta G°$, given by Alwan *et al.* (*30*) for the Cu,Zn hydroxycarbonates. The other endothermic peak (T''_{max} in Table 1) appearing in the DTA thermograms for the biphasic systems may surely be assigned to the decomposition of aurichalcite. The presence of a copper hydrozincite phase can be disregarded in these samples since the T'' maximum is in the range 593–613 K, whereas the maximum peak temperature for pure hydrozincite (T'''_{max} in Table 1) is found at a much lower temperature, 518 K, in agreement with the decomposition temperature of 503 K given for this mineral (*27*). Furthermore, it may be noticed that T'' is almost coincident with the DSC peak maximum temperature found by Petrini *et al.* (*11*) for the sample at Cu/Zn = 30/70 and which, from our results, is attributable to an aurichalcite-like phase decomposition. A semiquantitative DTA analysis of the relative amounts of zincian–malachite and aurichalcite present in the 77/23, 67/33, and 50/50 precursors gave good reproducibility with the XRD results, as shown in Table 1.

It may finally be added that preliminary X-ray photoelectron spectroscopy (XPS) investigations have shown that both in the monophasic and biphasic samples, the surface Cu/Zn atomic ratios are nearly equal to those found by chemical analysis. This fact suggests that there is a homogeneous dispersion of zinc in the solid solutions and a good interdispersion of the zincian–malachite and aurichalcite phases. A comparative study of the photoelectron and X-ray excited Auger transitions of copper and zinc gives support for an increasing covalency of the chemical bonds in zincian–malachite with respect to pure malachite. The XPS study of the precursors and of the calcined and reduced oxide catalysts will be the object of a forthcoming paper.

REFERENCES

1. Klier, K., *in* "Advances in Catalysis" (D. D. Eley, H. Pines and P. B. Weisz, Eds.), Vol. 31, p. 243, and references therein. Academic Press, New York, 1982.
2. Okamoto, Y., Fukino, K., Imanaka, T., and Teranishi, S., *J. Phys. Chem.* **87,** 3740 (1983).
3. Busetto, C., Del Piero, G., Manara, G., Trifirò, F., and Vaccari, A., *J. Catal.* **85,** 260 (1984).
4. Himelfarb, P. B., Simmons, G. W., Klier, K., and Herman, R. G., *J. Catal.* **93,** 442 (1985).
5. Natta, G., *in* "Catalysis" (P. H. Emmett, Ed.), Vol. 3, p. 349, and references therein. Reinhold, New York, 1955.
6. Klier, K., *Appl. Surf. Sci.* **19,** 267 (1984).
7. Parris, G. E., and Klier, K., *J. Catal.* **97,** 374 (1986).
8. Dominguez, E. J. M., Simmons, G. W., and Klier, K., *J. Mol. Catal.* **20,** 369 (1983).
9. Chinchen, G. C., Waugh, K. C., and Whan, D. A., *Appl. Catal.* **25,** 101 (1986).
10. Chinchen, G. C., and Waugh, K. C., *J. Catal.* **97,** 280 (1986).
11. Petrini, G., Montino, F., Bossi, A., and Garbassi, G., *in* "Studies in Surface Science and Catalysis, Preparation of Catalysts III" (G. Poncelet, P. Grange, and P. A. Jacobs, Eds.), Vol. 16, p. 735. Elsevier, Amsterdam, 1983.
12. Stacey, M. H., and Shannon, M., *in* "Reactivity of Solids (P. Barret and L. C. Dufour, Eds.), p. 713. Elsevier, Amsterdam, 1985.
13. Rasmussen, B. S., Højlund Nielsen, P. E., Villadsen, J., and Hansen, J. B., *in* "Preparation of Catalysts IV" (B. Delmon, P. Grange, P. A. Jacobs, and G. Poncelet, Eds.), p. 785. Elsevier, Amsterdam, 1987.
14. Jambor, J. L., and Pouliot, G., *Canad. Mineral.* **8,** 385 (1965); X-ray Powder Data File, ASTM 19-1458 (for hydrozincite) and ASTM 19-743 (for aurichalcite).
15. X-ray Powder Data File, ASTM 14-687.
16. X-ray Powder Data File, ASTM 18-1095.
17. X-ray Powder Data File, ASTM 10-399; Wells, A. F., *Acta Crystallogr.* **4,** 200 (1951).
18. Azaroff, L. V., and Buerger, M. J., "The Powder Method in X-ray Crystallography." McGraw-Hill, New York, 1958.
19. Jambor, J. L., *Geol. Surv. Canad.*, Report of Activities, Part C; paper 76-1C (1976).
20. Dunitz, J. D., and Orgel, L. E., *Nature (London)* **179,** 462 (1957).
21. Bragg, L., and Claringbull, G. F., "Crystal Structures of Minerals." Bell, London, 1965.

22. Shannon, R. D., *Acta Crystallogr. A* **32,** 751 (1976).
23. Ghose, S., *Acta Crystallogr.* **17,** 1051 (1964); Povarennykh, A. S., "Crystal Classification of Minerals," Vol. 2, p. 616. Plenum, New York, 1972.
24. Porta, P., and Mazzarano, A., in "Reactivity of Solids" (P. Barrett and L. C. Dufour, Eds.), p. 1053. Elsevier, Amsterdam, 1985.
25. Porta, P., and Anichini, A., *Z. Phys. Chem. Neue Folge* **127,** 233 (1981).
26. Goodenough, J. B., and Loeb, A. L., *Phys. Rev.* **98,** 391 (1955).
27. Dana's System of Mineralogy, 7th Ed., Vol. 2, p. 247. Wiley, New York, 1951.
28. Doesburg, E. B. M., Höppener, R. H., de Konig, B., Xiaoding, X., and Scholten, J. J. F., *in* "Preparation of Catalysts IV" (B. Delmon, P. Grange, P. A. Jacobs and G. Poncelet, Eds.), p. 767. Elsevier, Amsterdam, 1987.
29. Anufrienko, V. F., Yurieva, T. M., and Hadzieva, F. S., *React. Kinet. Catal. Lett.* **27,** 201 (1985).
30. Alwan, K. A., Thomas, J. H., and Williams, P. A., *Transition Met. Chem.* **5,** 3 (1980).